



# HHS Public Access

Author manuscript

*Eur Radiol.* Author manuscript; available in PMC 2017 December 29.

Published in final edited form as:

*Eur Radiol.* 2016 October ; 26(10): 3368–3376. doi:10.1007/s00330-015-4188-z.

## Amide Proton Transfer (APT) MR Imaging and Magnetization Transfer (MT) MR Imaging of Pediatric Brain Development

**Hong Zhang,**

Imaging Center, Department of Radiology, Beijing Children's Hospital, Capital Medical University, Beijing, China

**Huiying Kang,**

Imaging Center, Department of Radiology, Beijing Children's Hospital, Capital Medical University, Beijing, China

**Xuna Zhao,**

Philips Healthcare, Beijing, China

**Shanshan Jiang,**

Division of MR Research, Department of Radiology, Johns Hopkins University, Maryland, United States

**Yi Zhang,**

Division of MR Research, Department of Radiology, Johns Hopkins University, Maryland, United States

**Jinyuan Zhou, and**

Division of MR Research, Department of Radiology, Johns Hopkins University, Maryland, United States

**Yun Peng**

Imaging Center, Department of Radiology, Beijing Children's Hospital, Capital Medical University, Beijing, China

### Abstract

**Objectives**—To quantify the brain maturation process during childhood using combined APT and conventional MT imaging at 3 Tesla.

**Methods**—Eighty-two neurodevelopmentally normal children (44 males and 38 females; age range, 2–190 months) were imaged using an APT/MT imaging protocol with multiple saturation frequency offsets. The APT-weighted (APTW) and MT ratio (MTR) signals were quantitatively analyzed in multiple brain areas. Age-related changes in MTR and APTW were evaluated with a non-linear regression analysis.

---

Corresponding authors: Yun Peng, MD, PhD, Imaging Center, Department of Radiology, Beijing Children's Hospital, Capital Medical University, Beijing, China, Phone: (+86)139-1185-5572, ppengyun@yahoo.com or; Jinyuan Zhou, PhD, Division of MR Research, Department of Radiology, Johns Hopkins University, 600 N., Wolfe Street, Park 336, Baltimore, MD 21287, USA, Phone: (410) 955-7491, Fax: (410) 614-1977, jzhou@mri.jhu.edu.

**Results**—The APTW signals followed a decreasing exponential curve with age in all brain regions measured ( $R^2 = 0.7$ – $0.8$  for the corpus callosum, the frontal and occipital white matter, and the centrum semiovale). The most significant changes appeared within the first year. At maturation, larger decreases in APTW and lower APTW values were found in the white matter. On the contrary, the MTR signals followed an increasing exponential curve with age in the same brain regions measured, with the most significant changes appearing within the initial two years. There was an inverse correlation between the MTR and APTW signal intensities during brain maturation.

**Conclusions**—Together with MT imaging, protein-based APT imaging can provide additional information in assessing brain myelination in the paediatric population.

### Keywords

Brain maturation; myelination; amide proton transfer imaging; biomarker; MRI

---

### Introduction

Human brain development is a complicated and lifelong process, in which the creation of myelin (myelination) occurs between midgestation and the second postnatal year, and accompanies neuronal synaptogenesis, as well as gray and white matter growth [1-3]. MRI is the modality of choice for assessing normal as well as abnormal brain maturation [4, 5]. Commonly used pulse sequences are  $T_2$ -weighted,  $T_1$ -weighted, and diffusion-weighted MRI [6-9]. In recent decades, MRI has undergone a rapid evolution from structural to functional and molecular imaging. It has been reported that several advanced imaging techniques can provide additional information about brain maturation [10, 11]. For example, based on the diffusion-tensor imaging technique, multiple MRI parameters, such as apparent diffusion coefficients, fractional anisotropy, as well as axial and radial diffusivity, have been used to characterize the axonal organization and degree of myelination during brain development [12-14].

The well-known magnetization transfer (MT) contrast is based on the interaction between semi-solid macromolecular protons and the free water protons of tissue [15]. In the brain, the semi-solid macromolecules that contribute to the MT contrast include cholesterol and many other lipids [16]. The increased MT effect has been observed in the developing brain [17, 18]. These changes in MRI parameters are thought to result from myelination, and thus, they can be used to assess whether brain maturation is progressing normally. Amide proton transfer (APT) imaging [19] is a chemical exchange saturation transfer-based molecular MRI approach [20, 21], by which endogenous mobile proteins (such as those dissolved in the cytoplasm) can be detected [22]. It has been demonstrated recently that APT-weighted (APTW) signals, as image biomarkers, could examine the spatial extent and pathological grade of several human tumours due to increased mobile protein and peptide concentrations [23, 24], and tissue pH changes in stroke (where pH decreases) [25].

In our study, we explored the normal brain maturation in the paediatric population using conventional MT and APT imaging at 3T. The goal was to measure the age-dependent patterns of change in the protein-based APTW signals in different paediatric brain regions

and to evaluate their relationship to the conventional MTR signals in assessing the process of myelination. We hypothesize that the brain myelination process is associated with a decrease in the mobile protein content and an increase in the semi-solid macromolecular content, leading to both a decreasing APTW signal and an increasing MTR signal. A quantitative MRI biomarker at the molecular level during this conspicuous white matter maturation period is crucial to better understand the mechanisms of brain development and maturation, delayed development, and various neurologic diseases in the paediatric population.

## Materials and Methods

### Subjects

This study was approved by the local institutional review board. Written, informed consent was given by all the children's parents prior to participation to this study. The following criteria were used for inclusion of patients: between ages 0 and 18 years; full term (gestational age between 37 and 41 weeks) without any complicated perinatal courses; normal brain MR imaging results; normal myelination for the corresponding age; clearly normal results of the neurological examination; free of current and past neurological or psychiatric disorders; no evidence of genetic, metabolic, or infectious disorders. Between July 2012 and January 2014, 107 potential participants who were referred for neuroimaging for varied indications (the most common of which were dizziness, headaches, and idiopathic febrile seizures; see supplementary Table S1) were identified after a preliminary screening. To prove that the subjects were neurodevelopmentally normal, a paediatric neurologist performed a full neurological examination of each patient. The tests that were used were the Gesell Development Scale, the Wechsler Preschool and Primary Scale of Intelligence, and the Wechsler Intelligence Scale for Children. The developmental quotient/intelligence quotient was calculated in all children. Based on conventional MR images, a radiologist (Y.P., who had 11 years of experience in brain imaging) further assessed the images for the presence of disease and the degree of myelination, using the guidelines presented previously [6]. A follow-up review of the patients' medical records was performed at one year after the MR examination, and any children with demonstrated neurologic abnormalities or delays in developmental milestones were excluded.

Based on the inclusion criteria, 18 children were excluded from this study (13 children because of developmental delay; five children because of abnormal MRI results, such as Chiari malformation, Pineal cyst, and Rathke's cyst; see supplementary Table S1). In addition, data from seven children were further rejected because of insufficient image quality due to obvious motion artefacts. Finally, 82 children (42 males and 40 females; age range, 2–190 months; Table 1) with the normal brain development were included in this study. The mean developmental quotient/intelligence quotient score of the subjects was  $109.5 \pm 6.7$  (mean  $\pm$  standard deviation). Children younger than five years of age were sedated with oral 10% chloral hydrate (0.3–0.5ml/kg) before the MRI scans because of their young age.

## MRI Protocol

All subjects were imaged on a 3 Tesla MRI system (Achieva, Philips Medical Systems, Best, The Netherlands), using a dual-channel body coil for transmission and an eight-channel sensitivity-encoding coil for reception. Pencil-beam, second-order shimming was used. MT/APT imaging was incorporated into a standard clinical MRI examination protocol for the brain (field of view, 230 mm×190 mm; 18 slices; slice thickness, 5 mm; gap, 1 mm), including axial T<sub>2</sub>-weighted (repetition time, 3000 ms; echo time, 100 ms), T<sub>1</sub>-weighted (repetition time, 2308 ms; echo time, 13 ms), fluid-attenuated inversion recovery (FLAIR; repetition time, 7000 ms; echo time, 120 ms; inversion recovery time, 2200 ms), and diffusion-weighted (repetition time, 7000 ms; echo time, 120 ms; b factors, 0 and 1000 s/mm<sup>2</sup>).

MT/APT imaging was based on a pseudo-continuous wave radiofrequency irradiation (saturation duration, 200 ms×4; inter-pulse delay, 10 ms; block pulses; average power level, 2 μT), with a fat-suppressed, single-shot, turbo-spin-echo readout: repetition time, 3000 ms; turbo-spin-echo factor, 50; field of view, 230 mm×190 mm; matrix, 144×95, reconstructed to be 400×400; slice thickness, 5 mm. We used a multi-offset, multi-acquisition MT/APT imaging protocol. The 31 offsets used were: 0, ±0.25, ±0.5, ±0.75, ±1 (2), ±1.5 (2), ±2 (2), ±2.5 (2), ±3 (2), ±3.25 (2), ±3.5 (8), ±3.75 (2), ±4 (2), ±4.5, ±5, ±6, and 15.6 ppm (the values in parentheses are the number of acquisitions, which was one if not specified). An unsaturated image was acquired for the signal normalization. Three transverse slices of the head, including the pons, the basal ganglia, and the centrum semiovale, were acquired, and each of these three slices coincided exactly with one standard MRI slice acquired (T<sub>2</sub>-weighted, T<sub>1</sub>-weighted, FLAIR, and diffusion-weighted). The acquisition time was about two minutes 40 seconds per slice. The duration of a complete MR examination was 15–20 minutes.

## Image Processing and Analysis

The image analysis was performed using the Interactive Data Language (IDL; ITT Visual Information Solutions, Boulder, CO, USA). To reduce possible motion artefacts during the scanning, the acquired MT/APT image series for each slice was registered to the saturated image at 3.5 ppm [26], which was first registered with the corresponding slice on the standard MRI images acquired. The registration was performed with the analysis of functional neuroimages software (AFNI [27]; NIH/NIMH, Bethesda, MD, USA), using a rigid-body transformation of three degrees of freedom. The measured MT spectra ( $S_{\text{sat}}/S_0$ , in which  $S_{\text{sat}}$  and  $S_0$  are the signal intensities with and without selective radiofrequency irradiation, plotted as a function of saturation frequency offset, relative to water) were corrected for B<sub>0</sub> field heterogeneity effects on a pixel-by-pixel basis, as described in the literature [28]. The magnetization transfer ratio (MTR) was defined according to the equation:  $\text{MTR} = 1 - S_{\text{sat}}/S_0$ . Conventional MTR images were calculated with the saturated images at 15.6 ppm (2 kHz). APT imaging was quantified through the standard MTR asymmetry (MTR<sub>asym</sub>) analysis with respect to the water resonance, and the calculated MTR<sub>asym</sub>(3.5ppm) images were called APTW images [23].

The acquired MR images were reviewed by two radiologists (H.Z. and Y.P., who had six and 11 years of experience in brain imaging, respectively), and the quantitative image analysis was further performed. Ten regions of interest were manually drawn, in consensus, using the co-registered standard MR images (T<sub>2</sub>-weighted or FLAIR) as the anatomical reference (Fig. 1): pons; middle cerebellar peduncle; genu of the corpus callosum; splenium of the corpus callosum; frontal white matter; occipital white matter; caudate, putamen; thalamus; and centrum semiovale. Similar to the previous MT studies of the developing brain [17, 18], the change in MTR(15.6ppm signal intensities with age was fitted by a single exponential function:  $y = a_1 - b_1 \cdot \exp(-x/c_1)$ , while the change in APTW signal intensities with age was fitted by a single exponential function:  $y = a_2 + b_2 \cdot \exp(-x/c_2)$ .

### Statistical Analysis

All data were analyzed using the statistical package SPSS for Windows (Version 17.0, Chicago, IL). The MTR/APTW imaging intensities [MTR(15.6ppm), MTR<sub>asym</sub>(3.5ppm)] were reported for each region in all subjects. Left-right hemispheric differences in MTR or APTW were tested with a paired Student's t-test. As there were no significant hemispheric differences, data from the left and right hemispheres for each subject were combined for analysis. Age-related changes in MTR and APTW for each region were evaluated by a non-linear regression analysis. Three regression model parameters ( $a_1$ ,  $b_1$ , and  $c_1$  for MTR;  $a_2$ ,  $b_2$ , and  $c_2$  for APTR) were obtained, and goodness-of-fit was estimated using an R<sup>2</sup> value. An unpaired Student's t-test was used to compare differences between the regression parameters for the white matter and the basal ganglia. Statistical significance was accepted at  $p < 0.05$ .

### Results

Figure 2 shows the MTR/age data-fitting curves, and Table 2 summarizes the fitted parameters for the different brain structures in 82 neurodevelopmentally normal children. Higher R<sup>2</sup> values above 0.5 were obtained in all brain regions measured (particularly in the corpus callosum, the frontal and occipital white matter, as well as the centrum semiovale, R<sup>2</sup> = 0.8–0.9), indicating that the model function fitted the MTR data well. The MTR followed an increasing exponential curve with age, with the most significant changes appearing within the initial two years. Figure 3 showed the APTW/age data-fitting curves, and Table 3 summarizes the fitted parameters for the different brain structures in 82 neurodevelopmentally normal children. Although the pons, the caudate, the putamen, and the thalamus appeared to have a relatively poor goodness-of-fit (R<sup>2</sup> ≈ 0.2) to the exponential model, the other structures fitted the model reasonably well (R<sup>2</sup> = 0.7–0.8 for the corpus callosum, the frontal and occipital white matter, as well as the centrum semiovale). The APTW followed a decreasing exponential curve with age, with the most significant changes seemingly appearing within the first year.

Based on the fitting, at birth, the highest MTR values ( $a_1 - b_1$  in Table 2) and the lowest APTW values ( $a_2 + b_2$  in Table 3) were found in the pons, the middle cerebellar peduncle, and the thalamus. The lowest MTR values and the highest APTW values were found in the corpus callosum, the frontal and occipital white matter, and the centrum semiovale. After

brain myelination, the highest MTR values (“ $a_1$ ” in Table 2) and the lowest APTW values (“ $a_2$ ” in Table 3) were measured in the corpus callosum and some other white matter structures, while the lowest MTR values and the highest APTW values were measured in the caudate, the putamen, and the thalamus. Note that the pons had both high MTR and APTW values, and the middle cerebellar peduncle had high MTR values and intermediate APTW values. Larger increases in MTR (“ $b_1$ ” in Table 2) and the higher MTR values at maturation (“ $a_1$ ” in Table 2) were found in the white matter structures (the corpus callosum, the frontal and occipital white matter, and the centrum semiovale) rather than in the basal ganglia ( $p < 0.001$  and  $0.05$ , respectively). In addition, larger decreases in APTW (“ $b_2$ ” in Table 3) and the lower APTW values at maturation (“ $a_2$ ” in Table 3) were found in the white matter structures rather than in the basal ganglia (both  $p < 0.001$ ).

Based on the fitted equations, parameter “ $c_{1,2}$ ” indicates the rate of the change: a low “ $c_1$ ” value corresponding to a quick increase in MTR and a low “ $c_2$ ” value corresponding to a quick decrease in APTW. According to Tables 2 and 3, it can be seen that the lowest “ $c_{1,2}$ ” values were measured in the caudate and the putamen (eight months for MTR, four-to-five months for APTW), while the highest “ $c_{1,2}$ ” values were found in the pons and the middle cerebellar peduncles (23–26 months for MTR, 12 months for APTW). Notably, the “ $c_1$ ” values associating with the MTR-age dependency were significantly higher ( $p = 0.001$ ) than the “ $c_2$ ” values associating with the APTW-age dependency, suggesting that the decrease in APTW (“ $c_2$ ” range, four-12 months, namely, within the first year) was faster than the increase in MTR (“ $c_1$ ” range, eight-26 months, namely, within the initial two years) in all regions of interest.

Figures 4 and 5 show the representative  $T_2$ -weighted images, MTR images, and APTW images acquired from a pair of neurodevelopmentally normal children of three months old vs. 155 months old. Based on Fig. 4, the MTR signal intensities increased in the white matter structures and the basal ganglia with age, while the APTW signal intensities decreased in these brain regions with age. Based on Fig. 5, the MTR signal intensities increased in the centrum semiovale with age, while the APTW signal intensities decreased in the centrum semiovale with age. Relatively large changes in MTR and APTW can be seen in all white matter structures where myelination occurred.

## Discussion

In this study, we have demonstrated the feasibility and values of using the MTR and APTW MRI signals as imaging biomarkers to assess paediatric brain development. Our examination revealed that the MTR signals followed an increasing exponential curve with age, as reported before [17, 18], whereas the APTW signals followed a decreasing exponential curve with age. There was an inverse correlation between the MTR and APTW changes during brain maturation. At maturation, larger increases in MTR and higher MTR values, and larger decreases in APTW and lower APTW values were found in the white matter. The low  $R^2$  values were obtained for MTR in basal ganglia and for APTW in basal ganglia and pons, due to the relatively small change in MTR or APTW during the maturation process. The relatively higher MTR and relatively lower APTW fitted within the pons and middle cerebellar peduncle at birth may be associated with a rapid maturation in these areas in the

last few weeks of pregnancy and in the first few weeks post-delivery, as reported in the literature [6, 17]. The fact that the MTR signals overall had a relatively better goodness-of-fit to the exponential model than the APTW signals shows that MTR is likely more sensitive to myelination than the APTW approach. On the other hand, our data showed that the decrease in APTW with age in the developmental process was more rapid than the increase in MTR with age. It was reported previously that the increase in MTR values was more rapid than the decrease in  $T_2$  values during brain development [17]. Therefore, the protein-based APTW signal is potentially a novel imaging biomarker for the early assessment of paediatric brain development.

Technically, conventional MT imaging (quantified by MTR) is sensitive to semi-solid macromolecules in the more solid environment of the cell (such as lipids and proteins in the myelin, membrane, and nucleus). Consistent with previous reports [17, 18], this study found that MTR increased with brain myelination, and the myelinated white matter had a higher MTR value than the deep gray matter, due to the increased content of semi-solid lipids (cholesterol, phospholipids, glycolipids) and structural proteins in myelinated neurons [10, 29]. On the other hand, APT imaging was designed to detect mobile proteins in biological tissues. In principle, if proteins are in a more liquid compartment within a cell, they have a specific amide proton resonance frequency at  $\sim 3.5$  ppm downfield from water, and could be potentially detected by APT MRI [22]. The myelin sheath is a multilamellar membrane tightly wrapped around the axons of neurons in the central and peripheral nervous systems [29, 30]. Previous polarized microscopy and radiographic diffraction experiments have shown that the myelin layers have a protein-lipid-protein-lipid-protein structure. It was estimated that proteins constitute  $\sim 30\%$  of the myelin dry weight in the central nervous system, and proteolipid protein ( $\sim 50\%$  of the myelin proteins) and myelin basic protein ( $\sim 30\text{--}40\%$  of the myelin proteins) are two major proteins in the myelin membrane. Developmental studies of immature oligodendrocytes have revealed that the myelin basic protein was detected in the oligodendroglial cytoplasm before the beginning of myelination and became most intense during early myelination [31, 32]. The decreasing protein mobility (from mobile proteins to semi-solid proteins, such as the shift of the myelin basic protein from the oligodendroglial cytoplasm to the myelin sheath) may explain the decreasing APTW signal intensity observed during brain myelination. The exact mechanism still requires a further study in the future.

There were some limitations to this study. First, myelination develops rapidly during the first months of life and is nearly completed by the end of the second year [1, 2]. Although little myelin exists in the brain at birth, subjects less than two months old should be included in future studies. The number of individuals of less than 2 years of age should also be increased to better evaluate the changes that happen in early life. Second, children younger than five years of age were sedated during the MRI scans to reduce possible motion artefacts. This sedative is safe and routinely used in clinical situations. It is possible that anaesthesia can alter MTR and APTW signals that are temperature-dependent, which was not evaluated in this study. However, the impact should be minimal [19] because the scanning time was short and the children were always kept warm during the scanning. Indeed, no unexpected changes were observed at five years of age in the measured MTR/age and APTW/age curves (Figs. 2 and 3). Third, only three brain slices were obtained because of the limitation of the

single-slice acquisition protocol. Thus, the MRI signal changes in other brain regions could not be evaluated in the present study. A fast and highly-sensitive, parallel transmission-based, three-dimensional APT technology that would be the choice for standardization on scanners from all manufactures may be used in the future [23, 33]. Forth, the resolution of APT-MRI sequence is relatively low. This can result in partial volume effects when drawing regions of interests on small structures, like corpus callosum in the first years/months. Finally, the standard APTW metric based on the MTR asymmetry analysis could be subject to contamination by the upfield nuclear Overhauser enhancement and other effects. To more accurately quantify the APT effect, a more complicated APT imaging acquisition [34, 35] or analysis [36-38] approach may be used in the future. However, it has been demonstrated recently that the MTR asymmetry at 3.5 ppm remains a valid metric for APT imaging at 3 T (clinical  $B_0$  field strengths) and 4.7 T [38].

In conclusion, the present study evaluated, for the first time, paediatric brain development with APT imaging. Our results have shown that the endogenous MTR and APTW signals are two promising, complementary imaging biomarkers by which to assess paediatric brain development at the molecular level. MTR followed an increasing exponential curve, while APTW followed a decreasing exponential curve with the myelination process, reflecting the interchange between the semi-solid and mobile macromolecular phases in tissue. At maturation, the myelinated white matter has a higher MTR value and a lower APTW value than the deep gray matter. The use of protein-based APT imaging has an additional value in assessing paediatric brain myelination, which may aid in the early detection of myelination disorders and in monitoring the effects of treatment in the clinic.

## Supplementary Material

Refer to Web version on PubMed Central for supplementary material.

## Acknowledgments

The authors thank Ms. Mary McAllister for editorial assistance. The scientific guarantor of this publication is Yun Peng, M.D., Ph.D. Dr. Jinyuan Zhou is a co-inventor on a patent at the US Patent and Trademark Office for the APT-MRI technology that is licensed to Philips Healthcare. This patent is owned and managed by Johns Hopkins University. The other authors of this manuscript declare no relationships with any companies, whose products or services may be related to the subject matter of the article. This study has received funding from the National Natural Science Foundation of China (31271161) and from the National Institutes of Health (R01NS083425, R01EB009731, and R01CA166171). No complex statistical methods were necessary for this paper. Institutional Review Board approval was obtained. Written informed consent was obtained from all subjects (patients) in this study. Methodology: prospective, diagnostic or prognostic study, performed at one institution.

## References

1. Brody BA, Kinney HC, Kloman AS, Gilles FH. Sequence of central nervous system myelination in human infancy. I. An autopsy study of myelination. *J Neuropathol Exp Neurol.* 1987; 46:283–301. [PubMed: 3559630]
2. Knickmeyer RC, Gouttard S, Kang C, et al. A structural MRI study of human brain development from birth to 2 years. *J Neurosci.* 2008; 28:12176–12182. [PubMed: 19020011]
3. Geng X, Gouttard S, Sharma A, et al. Quantitative tract-based white matter development from birth to age 2 years. *Neuroimage.* 2012; 61:542–557. [PubMed: 22510254]



4. Dietrich RB, Bradley WG, Zaragoza EJ, et al. MR evaluation of early myelination patterns in normal and developmentally delayed infants. *AJR Am J Roentgenol.* 1988; 150:889–896. [PubMed: 2450448]
5. Bird CR, Hedberg M, Drayer BP, Keller PJ, Flom RA, Hodak JA. MR assessment of myelination in infants and children: usefulness of marker sites. *AJNR Am J Neuroradiol.* 1989; 10:731–740. [PubMed: 2505502]
6. Barkovich AJ, Kjos BO, Jackson DE Jr, Norman D. Normal maturation of the neonatal and infant brain: MR imaging at 1.5 T. *Radiology.* 1988; 166:173–180. [PubMed: 3336675]
7. Ballesteros MC, Hansen PE, Soila K. MR imaging of the developing human brain. Part 2. Postnatal development. *Radiographics.* 1993; 13:611–622. [PubMed: 8316668]
8. Ding XQ, Kucinski T, Wittkugel O, et al. Normal brain maturation characterized with age-related T2 relaxation times: an attempt to develop a quantitative imaging measure for clinical use. *Invest Radiol.* 2004; 39:740–746. [PubMed: 15550835]
9. Forbes KP, Pipe JG, Bird CR. Changes in brain water diffusion during the 1st year of life. *Radiology.* 2002; 222:405–409. [PubMed: 11818606]
10. Laule C, Vavasour IM, Kolind SH, et al. Magnetic resonance imaging of myelin. *Neurotherapeutics.* 2007; 4:460–484. [PubMed: 17599712]
11. Welker KM, Patton A. Assessment of normal myelination with magnetic resonance imaging. *Semin Neurol.* 2012; 32:15–28. [PubMed: 22422203]
12. Sowell ER, Peterson BS, Thompson PM, Welcome SE, Henkenius AL, Toga AW. Mapping cortical change across the human life span. *Nature Neurosci.* 2003; 6:309–315. [PubMed: 12548289]
13. Deoni SC, Mercure E, Blasi A, et al. Mapping infant brain myelination with magnetic resonance imaging. *J Neurosci.* 2011; 31:784–791. [PubMed: 21228187]
14. Huang H, Shu N, Mishra V, et al. Development of human brain structural networks through infancy and childhood. *Cereb Cortex.* 2013; doi: 10.1093/cercor/bht1335
15. Henkelman RM, Stanisz GJ, Graham SJ. Magnetization transfer in MRI: a review. *NMR Biomed.* 2001; 14:57–64. [PubMed: 11320533]
16. Kucharczyk W, Macdonald PM, Stanisz GJ, Henkelman RM. Relaxation and magnetization transfer of white matter lipids at MR imaging: importance of cerebroside and pH. *Radiology.* 1994; 192:521–529. [PubMed: 8029426]
17. Engelbrecht V, Rassek M, Preiss S, Wald C, Modder U. Age-dependent changes in magnetization transfer contrast of white matter in the pediatric brain. *AJNR Am J Neuroradiol.* 1998; 19:1923–1929. [PubMed: 9874548]
18. van Buchem MA, Steens SC, Vrooman HA, et al. Global estimation of myelination in the developing brain on the basis of magnetization transfer imaging: a preliminary study. *AJNR Am J Neuroradiol.* 2001; 22:762–766. [PubMed: 11290496]
19. Zhou J, Payen J, Wilson DA, Traystman RJ, van Zijl PC. Using the amide proton signals of intracellular proteins and peptides to detect pH effects in MRI. *Nature Med.* 2003; 9:1085–1090. [PubMed: 12872167]
20. Zhou J, van Zijl PC. Chemical exchange saturation transfer imaging and spectroscopy. *Progr NMR Spectr.* 2006; 48:109–136.
21. Sherry AD, Woods M. Chemical exchange saturation transfer contrast agents for magnetic resonance imaging. *Annu Rev Biomed Eng.* 2008; 10:391–411. [PubMed: 18647117]
22. Yan K, Fu Z, Yang C, et al. Assessing amide proton transfer (APT) MRI contrast origins in 9L gliosarcoma in the rat brain using proteomic analysis. *Mol Imaging Biol.* 2015; doi: 10.1007/s11307-11015-10828-11306
23. Zhou J, Zhu H, Lim M, et al. Three-dimensional amide proton transfer MR imaging of gliomas: Initial experience and comparison with gadolinium enhancement. *J Magn Reson Imaging.* 2013; 38:1119–1128. [PubMed: 23440878]
24. Jiang S, Yu H, Wang X, et al. Molecular MRI differentiation between primary central nervous system lymphomas and high-grade gliomas using endogenous protein-based amide proton transfer MR imaging at 3 Tesla. *Eur Radiol.* 2015; doi: 10.1007/s00330-00015-03805-00331
25. Harston GW, Tee YK, Blockley N, et al. Identifying the ischaemic penumbra using pH-weighted magnetic resonance imaging. *Brain.* 2015; 138:36–42. [PubMed: 25564491]

26. Zhang Y, Heo HY, Lee DH, et al. Selecting the reference image for registration of CEST series. *J Magn Reson Imaging*. 2015; doi: 10.1002/jmri.25027
27. Cox RW. AFNI: software for analysis and visualization of functional magnetic resonance neuroimages. *Comput Biomed Res*. 1996; 29:162–173. [PubMed: 8812068]
28. Wen Z, Hu S, Huang F, et al. MR imaging of high-grade brain tumors using endogenous protein and peptide-based contrast. *Neuroimage*. 2010; 51:616–622. [PubMed: 20188197]
29. Barkovich AJ. Concepts of myelin and myelination in neuroradiology. *AJNR Am J Neuroradiol*. 2000; 21:1099–1109. [PubMed: 10871022]
30. Rispoli P, Carzino R, Svaldo-Lanero T, et al. A thermodynamic and structural study of myelin basic protein in lipid membrane models. *Biophys J*. 2007; 93:1999–2010. [PubMed: 17513373]
31. Sternberger NH, Itoyama Y, Kies MW, Webster Hd. Immunocytochemical method to identify basic protein in myelin-forming oligodendrocytes of newborn rat C.N.S. *J Neurocytol*. 1978; 7:251–263. [PubMed: 349119]
32. Hartman BK, Agrawal HC, Kalmbach S, Shearer WT. A comparative study of the immunohistochemical localization of basic protein to myelin and oligodendrocytes in rat and chicken brain. *J Comp Neurol*. 1979; 188:273–290. [PubMed: 91628]
33. Keupp, J., Baltes, C., Harvey, PR., van den Brink, J. Proc 19th Annual Meeting. ISMRM; Montreal, Quebec: 2011. Parallel RF transmission based MRI technique for highly sensitive detection of amide proton transfer in the human brain; p. 710
34. Zu Z, Janve VA, Xu J, Does MD, Gore JC, Gochberg DF. A new method for detecting exchanging amide protons using chemical exchange rotation transfer. *Magn Reson Med*. 2013; 69:637–647. [PubMed: 22505325]
35. Lee JS, Xia D, Ge Y, Jerschow A, Regatte RR. Concurrent saturation transfer contrast in in vivo brain by a uniform magnetization transfer MRI. *Neuroimage*. 2014; 95:22–28. [PubMed: 24662575]
36. Desmond KL, Moosvi F, Stanisz GJ. Mapping of amide, amine, and aliphatic peaks in the CEST spectra of murine xenografts at 7 T. *Magn Reson Med*. 2014; 71:1841–1853. [PubMed: 23801344]
37. Cai K, Singh A, Poptani H, et al. CEST signal at 2ppm (CEST@2ppm) from Z-spectral fitting correlates with creatine distribution in brain tumor. *NMR Biomed*. 2015; 28:1–8. [PubMed: 25295758]
38. Heo HY, Zhang Y, Jiang S, Lee DH, Zhou J. Quantitative assessment of amide proton transfer (APT) and nuclear Overhauser enhancement (NOE) imaging with extrapolated semi-solid magnetization transfer reference (EMR) signals: II. Comparison of three EMR models and application to human brain glioma at 3 T. *Magn Reson Med*. 2015; doi: 10.1002/mrm.25795

## Abbreviations

<b>APT</b>	amide proton transfer
<b>APTW</b>	APT-weighted
<b>FLAIR</b>	fluid-attenuated inversion recovery
<b>MT</b>	magnetization transfer
<b>MTR</b>	magnetization transfer ratio

### Key Points

- APTW signals followed a decreasing exponential curve with age
- The most significant APTW changes appeared within the first year
- At maturation, larger APTW decreases and lower APTW were found in WM
- MTR signals followed an increasing exponential curve with age

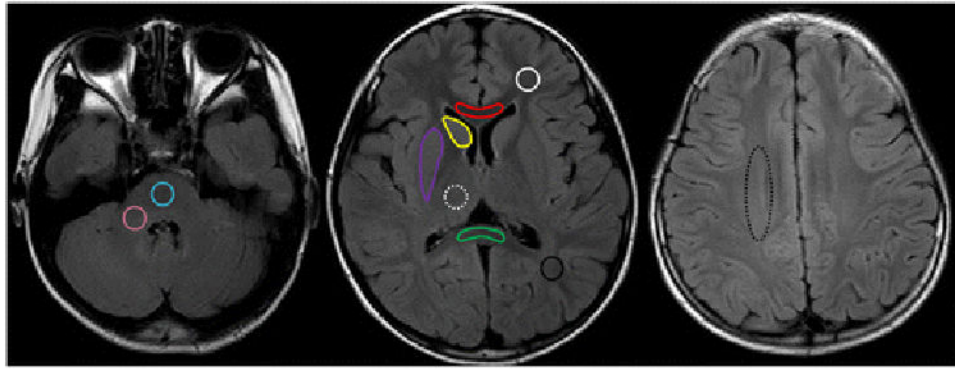


**Fig. 1.**

Examples of the definition of the regions of interest on the FLAIR images. The pons (blue), the middle cerebellar peduncle (pink), the genu of the corpus callosum (red), the splenium of the corpus callosum (green), the caudate (yellow), the putamen (purple), the thalamus (dashed white), the frontal white matter (solid white), the occipital white matter (solid black), and the centrum semiovale (dashed black) had median voxel numbers as follows: 151 (range, 127–185); 146 (range, 123–190); 98 (range, 74–109); 102 (range, 78–112); 105 (range, 82–128); 209 (range, 159–247); 160 (range, 128–190); 165 (range, 136–196); 133 (range, 102–167); and 358 (range, 304–389), respectively.

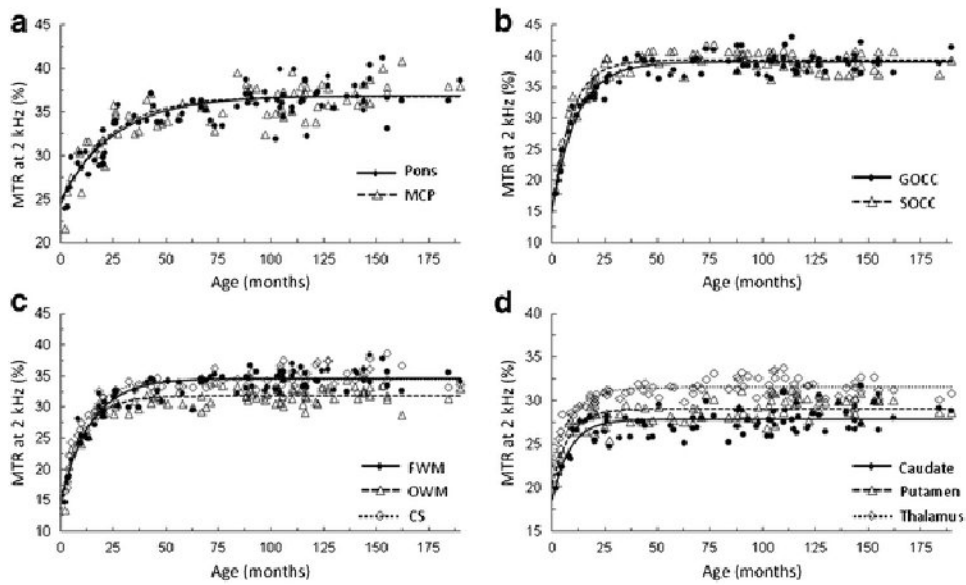


**Fig. 2.** Experimental and fitted age-related changes in the MTR values within the different brain regions in neurodevelopmentally normal children. **a** The pons ( $R^2 = 0.751$ ) and the middle cerebellar peduncle (MCP;  $R^2 = 0.752$ ); **b** the genu of the corpus callosum (GOCC;  $R^2 = 0.902$ ); the splenium of the corpus callosum (SOCC;  $R^2 = 0.889$ ); **c** the frontal white matter (FWM;  $R^2 = 0.861$ ); the occipital white matter (OWM;  $R^2 = 0.865$ ); the centrum semiovale (CS;  $R^2 = 0.845$ ); and **(d)** the caudate ( $R^2 = 0.511$ ), the putamen ( $R^2 = 0.566$ ), and the thalamus ( $R^2 = 0.715$ ).

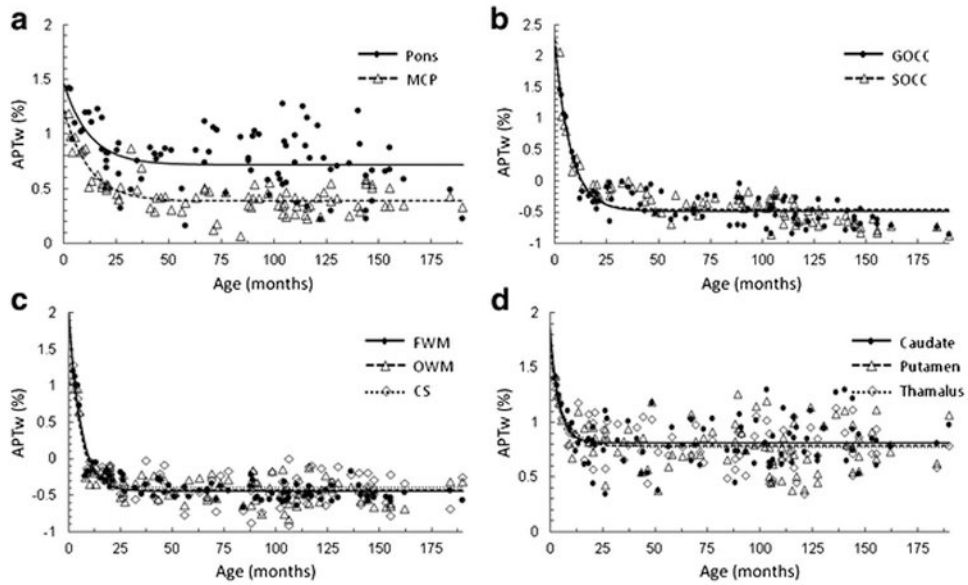


**Fig. 3.** Experimental and fitted age-related changes in the APTW values within the different brain regions in neurodevelopmentally normal children. **a** The pons ( $R^2 = 0.235$ ) and the middle cerebellar peduncle (MCP;  $R^2 = 0.641$ ); **b** the genu of the corpus callosum (GOCC;  $R^2 = 0.786$ ); the splenium of the corpus callosum (SOCC;  $R^2 = 0.734$ ); **c** the frontal white matter (FWM;  $R^2 = 0.874$ ); the occipital white matter (OWM;  $R^2 = 0.735$ ); the centrum semiovale (CS;  $R^2 = 0.685$ ); and **(d)** the caudate ( $R^2 = 0.222$ ), the putamen ( $R^2 = 0.188$ ), and the thalamus ( $R^2 = 0.221$ ).

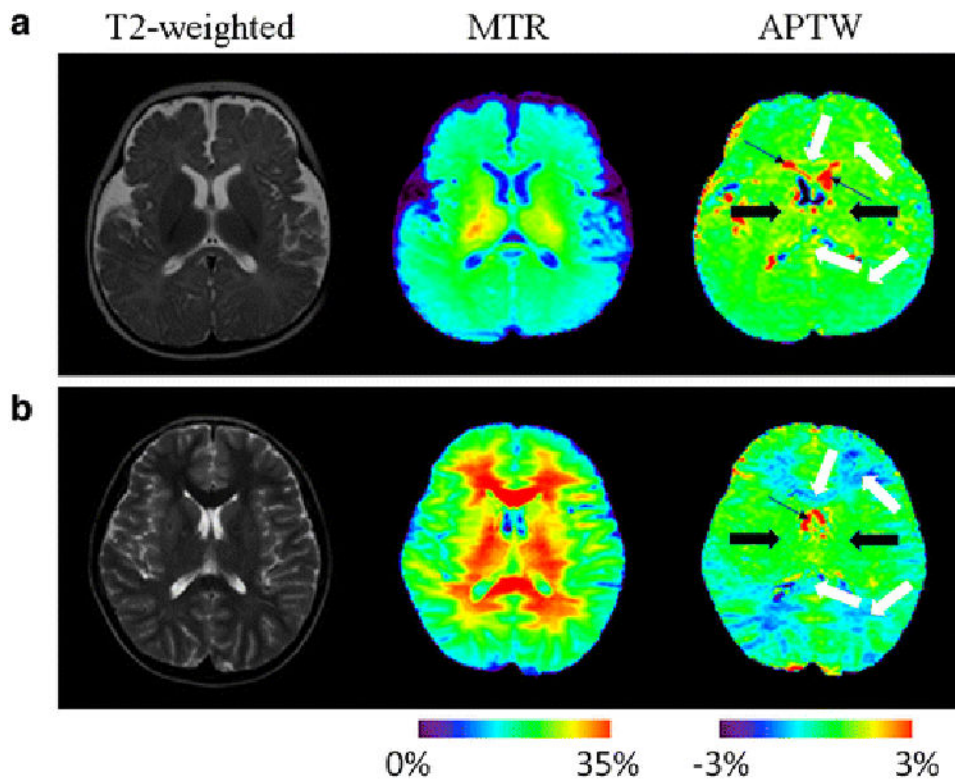


**Fig. 4.** T<sub>2</sub>-weighted images, MTR images, and APTW images of (a) a three-month-old neurodevelopmentally normal child and (b) a 155-month-old neurodevelopmentally normal child. With age, the MTR intensities increased, while the APTW intensities decreased in the white matter structures (white arrows) and in the basal ganglia (black thick arrows). Note the presence of CSF artefacts (black thin arrows). The changes were larger in the white matter structures than in the basal ganglia.

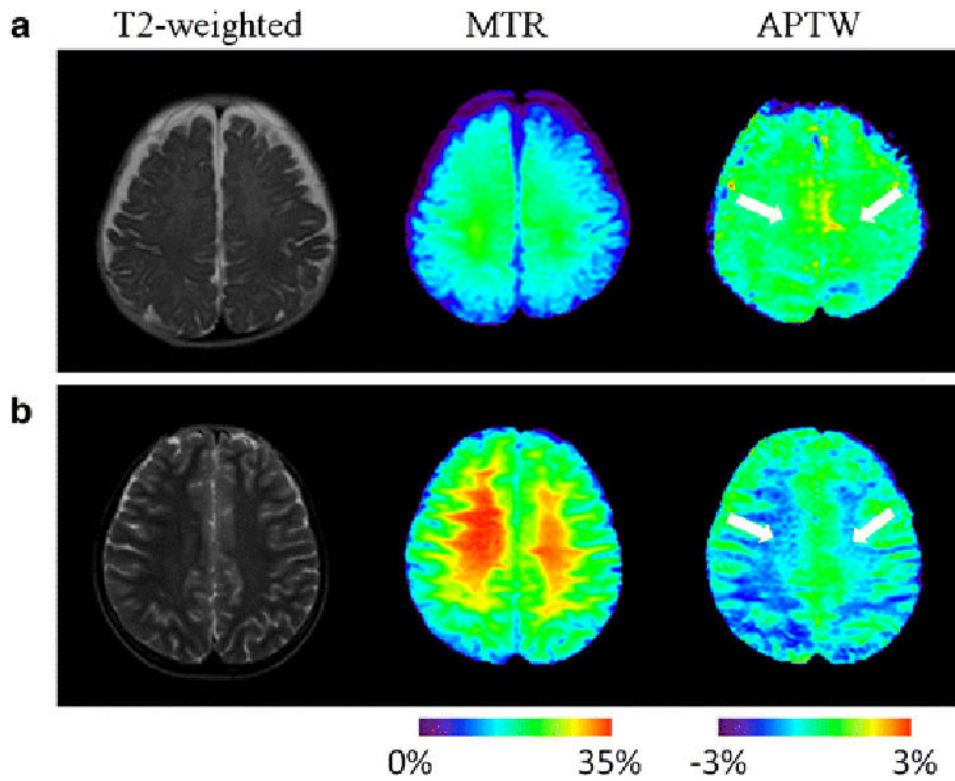


**Fig. 5.** T<sub>2</sub>-weighted images, MTR images, and APTW images of (a) a three-month-old neurodevelopmentally normal child and (b) a 155-month-old neurodevelopmentally normal child. With age, the MTR intensities increased, while the APTW intensities decreased in the centrum semiovale (white arrows).



**Table 1**  
**Age and gender distribution of neurodevelopmentally normal children recruited in this study**

Age range (years)	No. of Children (Male/Female)
0-2	16 (9/7)
2-4	9 (3/6)
4-7	13 (6/7)
7-10	24 (12/12)
10-16	20 (12/8)
Total	82 (42/40)

Author Manuscript

Author Manuscript

Author Manuscript

Author Manuscript

**Table 2**  
**Non-linear regression analysis of MTR values at 15.6 ppm (y) versus age (x) using the model  $y = a_1 - b_1 * \exp(-x/c_1)$**

ROI	$a_1 - b_1$ (%)	$a_1$ (%)	$b_1$ (%)	$c_1$ (month)	$R^2$
Pons	24.839	36.879	12.040	25.727	0.751
MCP	24.397	36.810	12.413	22.711	0.752
GOCC	15.584	39.044	23.460	11.905	0.902
SOCC	14.923	39.366	24.443	9.008	0.889
FWM	14.762	34.553	19.791	14.120	0.861
OWM	13.229	31.770	18.541	9.995	0.865
Caudate	18.616	27.848	9.232	8.373	0.511
Putamen	20.434	29.075	8.641	8.356	0.566
Thalamus	22.876	31.553	8.677	9.530	0.715
CS	14.77	34.499	19.729	11.160	0.845

MCP, middle cerebellar peduncle; GOCC, genu of the corpus callosum; SOCC, splenium of the corpus callosum; FWM, frontal white matter; OWM, occipital white matter; CS, centrum semiovale; (a1 – b1), the MTR value at birth; a1, the MTR value at maturation; b1, the amount of change during the maturation process; c1, the rate of change.

**Table 3**  
**Non-linear regression analysis of APTW values (y) versus age (x) using the model  $y = a_2 + b_2 \cdot \exp(-x/c_2)$**

ROI	$a_2+b_2$ (%)	$a_2$ (%)	$b_2$ (%)	$c_2$ (month)	$R^2$
Pons	1.457	0.722	0.735	12.111	0.235
MCP	1.214	0.387	0.827	11.811	0.641
GOCC	2.147	-0.485	2.632	7.651	0.786
SOCC	2.261	-0.454	2.715	7.047	0.734
FWM	2.022	-0.445	2.467	5.887	0.874
OWM	1.995	-0.434	2.429	5.213	0.735
Caudate	1.878	0.816	1.062	4.202	0.222
Putamen	1.675	0.789	0.886	4.701	0.188
Thalamus	1.449	0.774	0.675	7.371	0.221
CS	2.089	-0.399	2.488	5.195	0.685

MCP, middle cerebellar peduncle; GOCC, genu of the corpus callosum; SOCC, splenium of the corpus callosum; FWM, frontal white matter; OWM, occipital white matter; CS, centrum semiovale; ( $a_2 + b_2$ ), the APTW value at birth;  $a_2$ , the APTW value at maturation;  $b_2$ , the amount of change during the maturation process;  $c_2$ , the rate of change.